IEEE Access
Multidisciplinary | Rapid Review | Open Access Journal

Received September 24, 2019, accepted November 14, 2019, date of publication November 26, 2019,
date of current version December 13, 2019.

Digital Object Identifier 10.1109/ACCESS.2019.2956057

Preprocessed Method and Application of Magnetic Gradient Tensor Data

JINPENG LI, YINGTANG ZHANG, HONGBO FAN, AND ZHINING LI
Seventh Department, Army Engineering University, Shijiazhuang 050003, China
Corresponding author: Hongbo Fan (ffhhbboo@163.com)

ABSTRACT The edge detection method is significant in the interpretation of magnetic data, and can effectively identify the edge of the magnetic source. In this paper, a new edge detection method of magnetic sources is proposed under the oblique magnetization condition. First, the data of the magnetic field component is transformed into the total magnitude anomaly and its direction cosinesaccording to the inter-relationship between different magnetic field components. To eliminate noise, we use the K-Singular Value Decomposition denoising method based on the mean signal improvement to reconstruct the magnetic signal. Then, the three components of the magnetic field data is converted into the data of three components from the same magnetic source under the vertical magnetization condition by using the calculated magnetization direction of the magnetic source. Finally, the edge of the magnetic source is calculated through the ratio of the magnetic gradient tensor invariant to the B_{zz} component data under the vertical magnetization condition. This method is verified by simulation and experiment. The simulation and experimental results obtained show that this method considerably reduces the effects of the oblique magnetization. Besides, the method in this paper has high noise immunity.

INDEX TERMS Edge, K-singular value decomposition, magnetic gradient tensor invariant, oblique magnetization.

I. INTRODUCTION

In recent years, magnetic data interpretation based on magnetic gradient tensor plays an increasingly important role in military (unexploded ordnance detection), environment and resource exploration. Edge recognition is an important process for interpreting magnetic data, can make the physical edges of the magnetic sources be visualized. There are many methods to identify the edges of magnetic sources, such as Total horizontal derivative (THD), tilt angle, total horizontal derivative of the tilt angle, the theta map method [1]–[4].

However, in magnetic prospecting, the calculated edges by using the magnetic data of the oblique magnetization direction would cause the calculation result to be deviate from the edge of the actual magnetic source. References [5]–[7] show that the calculated edge is inconsistent with the actual edge under the oblique magnetization condition, especially when the inclination is equal to 45°. However, when the inclination is close to 0° or 90°, the identified edges are accurate. To deal with the influence of the oblique magnetization on the edge detection, researchers calculate the edge of the magnetic source mainly by two methods. The first method is to obtain magnetic measurement data or conversion data that is insensitive to the magnetization direction, and the data is calculated by using the edge calculation formula. The other method is that the magnetic measurement data is reduced to the pole; then, the calculated data is brought into the edge calculation formula. For the first method, researchers have proposed a series of calculation methods. Nabighian proposed the concept of two-dimensional analytical signal [8]. Roest et al. and Qin used the three-dimensional analytical signal of the magnetic anomaly to detect the edge of the geological body [9], [10]. The amplitude of the two-dimensional analytical signal is not affected by the magnetization direction. Meanwhile, the magnetization direction has little effect on the three-dimensional analytical signal, which is employed to the edge detection of the magnetic anomaly [11], [12]. Beiki et al. calculated the source location by using the normalized source strength [13], which is a rotational invariant derived from the eigenvalues of the magnetic gradient tensor matrix. Yin et al. defined the tilt angle using the normalized source strength to detect horizontal locations of magnetic sources [14]. However, the disadvantages of above methods are that the horizontal resolution of the edge detection result is

The associate editor coordinating the review of this manuscript and approving it for publication was Jenny Mahoney.

poor and the calculation result is greatly affected by the buried depth. For the second method, the magnetic data with high resolution could be used to perform the edge detection calculation without being constrained by the type of the calculation data. Nonetheless, the magnetic measurement data being reduced to the pole is needed in this method [5]–[7]. What's more, the descriptions of the specific calculation process in relevant reports were not detailed. In fact, the actual magnetization direction of the magnetic source must be known before the magnetic measurement data is reduced to the pole. Therefore, it is meaningful to estimate the actual magnetization direction of the magnetic source. In addition, noise is also an important factor in destroying the edge of the magnetic source.

In the present work, we have proposed a new edge detection method of magnetic sources under the oblique magnetization condition. We use the improved sparse representation method to reconstruct the magnetic signal in order to eliminate noise. And a correlation coefficient analysis is carried out to calculate the actual magnetization direction of the magnetic anomaly and we convert the three components of the magnetic field data into the data of three components from the same magnetic source under the vertical magnetization condition. We transform the data of magnetic field three components into magnetic gradient tensor. The edge of magnetic source is calculated by calculating the ratio of the magnetic gradient tensor invariant and the B_{zz} component data under the vertical magnetization condition.

The main plans of this paper are as follows. The preprocessed process of the magnetic gradient tensor and the edge detection method are described in the section 2. The calculation results of the simulation and experiment are described in the section 3. In the section 4, the conclusions of this paper are explained.

II. METHOD

A. MAGNETIC GRADIENT TENSOR

The positive direction of the x-axis is set to the north; the positive direction of the y-axis is set to the east; and the z-axis is set to the vertically down direction. The data of the magnetic gradient tensor is the spatial derivative of the magnetic field vector $\boldsymbol{B} = [B_x, B_y, B_z]^{\mathrm{T}}$ in three orthogonal directions along three coordinate axes. Therefore, the data of the magnetic gradient tensor at the observation point (x, y, z) can be expressed as:

$$\boldsymbol{\Gamma} = \begin{bmatrix} \partial/\partial x \\ \partial/\partial y \\ \partial/\partial z \end{bmatrix} \begin{bmatrix} B_x & B_y & B_z \end{bmatrix} = \begin{bmatrix} B_{xx} & B_{xy} & B_{xz} \\ B_{yx} & B_{yy} & B_{yz} \\ B_{zx} & B_{zy} & B_{zz} \end{bmatrix} \tag{1}$$

where $\boldsymbol{\Gamma}$ represents the magnetic gradient tensor matrix, B_{ij} $(i, j = x, y, z)$ represents the different magnetic gradient tensor component. And the magnetic gradient tensor matrix $\boldsymbol{\Gamma}$ is a symmetric matrix with five independent components B_{xx}, B_{xy}, B_{xz}, B_{yy}, B_{yz}. Therefore, all the components in the magnetic gradient tensor matrix $\boldsymbol{\Gamma}$ can be represented by these five independent components.

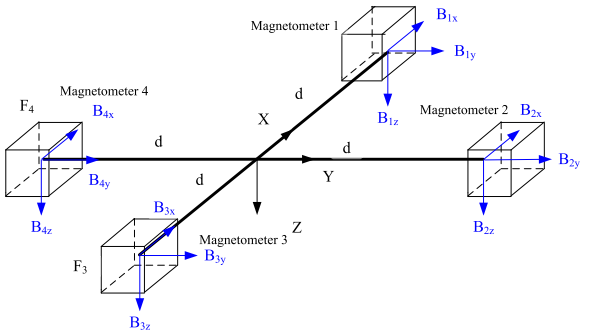

FIGURE 1. The planar cross-type magnetic gradient tensor detection system.

The eigenvalues of the magnetic gradient tensor matrix $\boldsymbol{\Gamma}$ are $\lambda_1, \lambda_2, \lambda_3$, where $\lambda_2 \leq \lambda_1, \lambda_2 \geq \lambda_3$. The normalized source strength (NSS) is defined as [15], [23]

$$\mathrm{NSS} = \left(-\lambda_2^2 - \lambda_1\lambda_3\right)^{1/2} \tag{2}$$

The NSS data is not affected by the magnetization direction in 2D case. Meanwhile, the magnetization direction has little effect on the NSS data in 3D case. It has a more effective judgment of the horizontal distribution position of the magnetic source. We can use the main positive value of the NSS data to determine the number of magnetic sources and divide into subareas that contain isolated magnetic source.

In the process of the actual measurement of the data of the magnetic gradient tensor, the test is carried out by using a planar cross-type magnetic gradient tensor detection system, which comprises four tri-axial fluxgate magnetometers placed on the measuring bracket, as shown in Fig. 1. The baseline distance between the two magnetometers is 2d, and the data of the magnetic gradient tensor obtained by the system can be expressed as:

$$\boldsymbol{\Gamma} = \begin{bmatrix} (B_{1x}-B_{3x})/2d & (B_{1y}-B_{3y})/2d & (B_{1z}-B_{3z})/2d \\ & (B_{2y}-B_{4y})/2d & (B_{2z}-B_{4z})/2d \\ & & -[(B_{1x}-B_{3x})/2d \\ & & +(B_{2y}-B_{4y})/2d] \end{bmatrix} \tag{3}$$

where B_{sv}, $s = 1, 2, 3$, $v = x, y, z$ is the magnetic field component in the vth direction measured by the sth magnetometer.

The structural errors of the planar cross-type magnetic gradient tensor detection system is expressed as [16] (4), as shown at the bottom of the next page where $\Delta\boldsymbol{\Gamma}$ is the structural errors of the planar cross-type magnetic gradient tensor detection system.

Through the error analysis of the magnetic gradient tensor system, it is known that the error between the actual measured value and the theoretical measured value is very small, which could be neglected.

B. PREPROCESSED METHOD OF THE DATA OF THE MAGNETIC GRADIENT TENSOR

1) K-SINGULAR VALUE DECOMPOSITION DENOISING METHOD BASED ON MEAN SIGNAL IMPROVEMENT

Since noise has a strong influence on the application of the data of the magnetic gradient tensor, reducing noise in the magnetic field data is needed. The method of sparse and redundant representations has been verified to effectively denoise images. The K-Singular Value Decomposition (KSVD) denoising model is described in literatures [17], [18]. In the denoising process of KSVD, it is required to assume that the noise is a zero-mean white Gaussian noise. However, this ideal situation does not exist in actual calculations. Therefore, we propose a KSVD denoising method based on the mean signal (KSVD-MS) improvement to reconstruct the magnetic data in this paper.

Above all, the mean value of the observed data $\boldsymbol{y} = [y_1, y_2, \ldots, y_i, \ldots, y_N]$ is calculated. Then, the mean value $\bar{\boldsymbol{y}} = [\bar{y}_1, \bar{y}_2, \ldots, \bar{y}_i, \ldots, \bar{y}_N]$ is segmented into the new mean signal $\boldsymbol{XM}$ and extended into the signal matrix $\boldsymbol{M}$ to form an expansion matrix $\boldsymbol{XY} = (\boldsymbol{M}, \boldsymbol{XM})$, where $\boldsymbol{M} = [M_1, M_2, \ldots, M_i, \ldots, M_N]$, $M_i = y_i - \bar{y}_i$, $\boldsymbol{XM}$ is the new mean signal by segmenting the mean data $\bar{\boldsymbol{y}}$ and $\boldsymbol{XY} = (\boldsymbol{M}, \boldsymbol{XM})$. When the mean signal is extended, the moving step of the sliding window is l, the size of the window is v, and $l < v$. It can be seen that the moving number of the sliding window is $t = \text{ceil}\left[(N - v)/l\right]$, where N is the number of the column of the observed data and ceil(x) represents the smallest integer greater than x. After that, KSVD denoising method is used to sparse the new mean signal $\boldsymbol{XM}$. Finally, the denoised signal $\boldsymbol{XM}'$ is obtained. The mean signal $\bar{\boldsymbol{y}}'$ is separated by the reverse order of previous steps.

2) THE DENOISING METHOD OF THE MEAN SIGNAL BASED ON MORPHOLOGICAL FILTER

As a kind of nonlinear filter based on mathematical morphology, the morphological filter is designed to form a probe, which is called structural element. The probe is used to match and locally correct the signal to achieve the purpose of extracting the edge contour of the signal and maintaining the main morphological characteristics of the signal. Therefore, the morphological filter is employed to denoise the mean signal $\bar{\boldsymbol{y}}'$. Besides, morphology has four basic operations: corrosion, expansion, morphological opening, and morphological closure [19].

Due to the anti-expansion of form opening and the scalability of form closure, there is a statistical offset phenomenon in the morphological filtering process, which impedes the noise suppression. It can be combined with open and closed operations to construct combined open-closed and closed-open filters (COOC), which can be defined as:

$$\text{COOC} = [\text{CO} + \text{OC}]/2 \tag{5}$$

where CO is the morphological closed-open filter and OC is the morphological open-closed filter.

The effect of morphological filters is not only related to the choice of morphological operations, but also closely related to the type and length of structural elements. Commonly used structural element types are linear, triangular, semi-circular, and sinusoidal. Engineering application experience shows that semi-circular structural elements filter random noise better, while triangular structure elements filter impulse noise better [20].

3) MAGNETIC DATA PROCESSING ALGORITHM

Noise denoising is primarily performed on a single component of the magnetic field; however, it does not simultaneously ensure the gradient accuracy of magnetic field components in different directions. In the calculation process, components of the magnetic field data are transformed into the total magnitude anomaly and its direction cosines to preserve the inter-relationship information between different magnetic field components while removing noises. The calculation procedures are shown as follows (see Fig. 2):

1. According to the vector synthesis principle of magnetic field, the total magnitude anomaly and its direction cosines can be expressed as:

$$\begin{cases} B = \left(|B_x|^2 + |B_y|^2 + |B_z|^2\right)^{1/2} \\ l = B_x/B, m = B_y/B, n = B_z/B \end{cases} \tag{6}$$

   where B is total magnitude anomaly; l, m and n are direction cosines of the total magnitude anomaly and three directions of the coordinate axis.
2. The expanded matrix obtained is separated into the signal matrix $\boldsymbol{M}'$ and the mean data $\bar{\boldsymbol{y}}'$ using the KSVD denoising method based on the mean signal improvement.
3. The residual signal $\overline{\boldsymbol{y}_1} = \bar{\boldsymbol{y}} - \bar{\boldsymbol{y}}'$ is calculated. Then the noise is reduced by using the morphological filter

$$\Delta\boldsymbol{\Gamma} = \begin{Bmatrix} \left.\frac{1}{3!}\frac{\partial^3 B_x}{\partial x^3}\right|_o \cdot d^2 & \left.\frac{1}{3!}\frac{\partial^3 B_x}{\partial y^3}\right|_o \cdot d^2 & \left.\frac{1}{3!}\frac{\partial^3 B_z}{\partial x^3}\right|_o \cdot d^2 \\ \left.\frac{1}{3!}\frac{\partial^3 B_y}{\partial x^3}\right|_o \cdot d^2 & \left.\frac{1}{3!}\frac{\partial^3 B_y}{\partial y^3}\right|_o \cdot d^2 & \left.\frac{1}{3!}\frac{\partial^3 B_z}{\partial y^3}\right|_o \cdot d^2 \\ \left.\frac{1}{3!}\frac{\partial^3 B_z}{\partial x^3}\right|_o \cdot d^2 & \left.\frac{1}{3!}\frac{\partial^3 B_z}{\partial y^3}\right|_o \cdot d^2 & \frac{-1}{3!}\left(\left.\frac{\partial^3 B_x}{\partial x^3}\right|_o + \left.\frac{\partial^3 B_y}{\partial y^3}\right|_o\right) \cdot d^2 \end{Bmatrix} \tag{4}$$

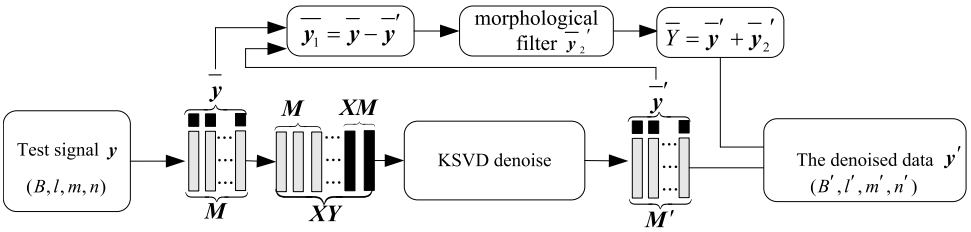

FIGURE 2. The chart of denoising procedure.

denoising method to obtain $\overline{y}_2'$. Therefore, the new mean data is $\overline{Y} = \overline{y}' + \overline{y}_2'$, the denoised data can be defined as:

$$y' = M' + \overline{Y}' \tag{7}$$

where $\overline{Y}' = \begin{bmatrix} \overline{Y}_1, \overline{Y}_2, \ldots, \overline{Y}_N \\ \cdots \\ \overline{Y}_1, \overline{Y}_2, \ldots, \overline{Y}_N \end{bmatrix}_{M \times N}$.

4. The total magnitude anomaly $\boldsymbol{B}$ and its direction cosines ($\boldsymbol{l}$, $\boldsymbol{m}$, $\boldsymbol{n}$) are denoised by using the above denoising method, and the denoised total magnitude anomaly $\boldsymbol{B}'$ and its direction cosines ($\boldsymbol{l}', \boldsymbol{m}', \boldsymbol{n}'$) are inversely reconstructed according to the (6).

$$\begin{bmatrix} \boldsymbol{B}_x' \\ \boldsymbol{B}_y' \\ \boldsymbol{B}_z' \end{bmatrix} = \left[\boldsymbol{B}' \Big/ \left(\boldsymbol{l}'^2 + \mathbf{m}'^2 + \mathbf{n}'^2 \right)^{1/2} \right] \begin{bmatrix} \boldsymbol{l}' \\ \boldsymbol{m}' \\ \boldsymbol{n}' \end{bmatrix} \tag{8}$$

where $\boldsymbol{B}_x'$, $\boldsymbol{B}_y'$, $\boldsymbol{B}_z'$ are denoised components of magnetic field.

C. APPLICATION OF MAGNETIC GRADIENT TENSOR IN MAGNETIC SOURCE EDGE DETECTION

1) THE TRANSFORMATION OF THE DATA OF MAGNETIC GRADIENT TENSOR

The calculated edges by using the magnetic data of the oblique magnetization direction will cause the calculation results to be deviate from the edges of the actual magnetic sources. In order to solve this problem, we convert the magnetic gradient tensor into the magnetic gradient tensor data of the same magnetic source that is under the vertical magnetization condition. The specific calculation processes are as follows:

Firstly, a series of inclination and declination values are selected, and we use the selected magnetization direction to calculate the reduced-to-the-pole (RTP) of the total magnetic intensity (TMI). The cross-correlation coefficient between the NSS and the TMI transformed data in different magnetization directions is calculated. The magnetization direction corresponding to the maximum value of the cross-correlation coefficient is the estimated magnetization direction. The cross-correlation can be expressed as [21]

$$C = \sum_{i=1}^{M} \sum_{j=1}^{N} (\Delta \mathrm{T_{rtp}}(i,j) - \overline{\Delta \mathrm{T_{rtp}}})(\mu(i,j) - \overline{\mu}) \Big/ \left(\sum_{i=1}^{M} (\Delta \mathrm{T_{rtp}}(i,j) - \overline{\Delta \mathrm{T_{rtp}}})^2 \sum_{j=1}^{N} (\mu(i,j) - \overline{\mu})^2 \right)^{1/2} \tag{9}$$

where M is the number of grids along the x-axis direction, N is the number of grids along the y-axis direction, and $\Delta \mathrm{T_{rtp}}$ is the RTP of the TMI, μ is the NSS data, $\overline{\Delta \mathrm{T_{rtp}}}$ is the average of the RTP of the TMI, and $\overline{\mu}$ is the average of the NSS data.

Then, the TMI is polarized according to the obtained magnetization direction. On the condition of frequency domain, the pole factor of the TMI is:

$$W(\mathrm{k_x}, \mathrm{k_y}) = K^2 \Big/ [K \sin \mathrm{I_0} + i \cos \mathrm{I_0}(k_x \cos \mathrm{D_0} + \mathrm{k}_y \sin \mathrm{D_0})] \cdot 1 \Big/ [K \sin I_1 + i \cos I_1(\mathrm{k_x} \cos D_1 + \mathrm{k_y} \sin D_1)] \tag{10}$$

where $\mathrm{k_x}$ is the wavenumber in the x-direction, $\mathrm{k_y}$ is the wavenumber in the y-direction, $K = \left(\mathrm{k_x^2} + \mathrm{k_y^2} \right)^{1/2}$. $\mathrm{I_0}$ is the inclination of geomagnetic background field, $\mathrm{D_0}$ is the declination of geomagnetic background field, $\mathrm{I_1}$ is the actual inclination of magnetic source and $\mathrm{D_1}$ is the actual declination of magnetic source.

Assuming $\mathrm{k_x} = r \cos\theta$, $\mathrm{k_y} = r \sin\theta$, $\theta = \arctan\left(\mathrm{k_x}/\mathrm{k_y}\right)$, $r = \left(\mathrm{k_x^2} + \mathrm{k_y^2} \right)^{1/2}$, then we convert the (10) to a conversion factor in polar form:

$$W(r,\theta) = 1 \Big/ [i \cos \mathrm{I_0} \cos(\theta - \mathrm{D_0}) + \sin \mathrm{I_0}] \cdot 1 \Big/ [i \cos \mathrm{I_1} \cos(\theta - \mathrm{D_1}) + \sin \mathrm{I_1}] \tag{11}$$

Now, according to the Fourier transform formula of the three components of the magnetic field data, the three-component data can be converted into the data of the same magnetic source that is under the vertical magnetization condition [22], [23].

2) THEORY OF MAGNETIC GRADIENT TENSOR INVARIANT EDGE DETECTION

The formula of magnetic gradient tensor invariant I is defined as:

$$I = B_{xx}B_{yy} + B_{yy}B_{zz} + B_{xx}B_{zz} - B_{xy}^2 - B_{xz}^2 - B_{yz}^2 \tag{12}$$

The method of magnetic gradient tensor invariant edge detection (IED) uses the magnetic gradient tensor invariant

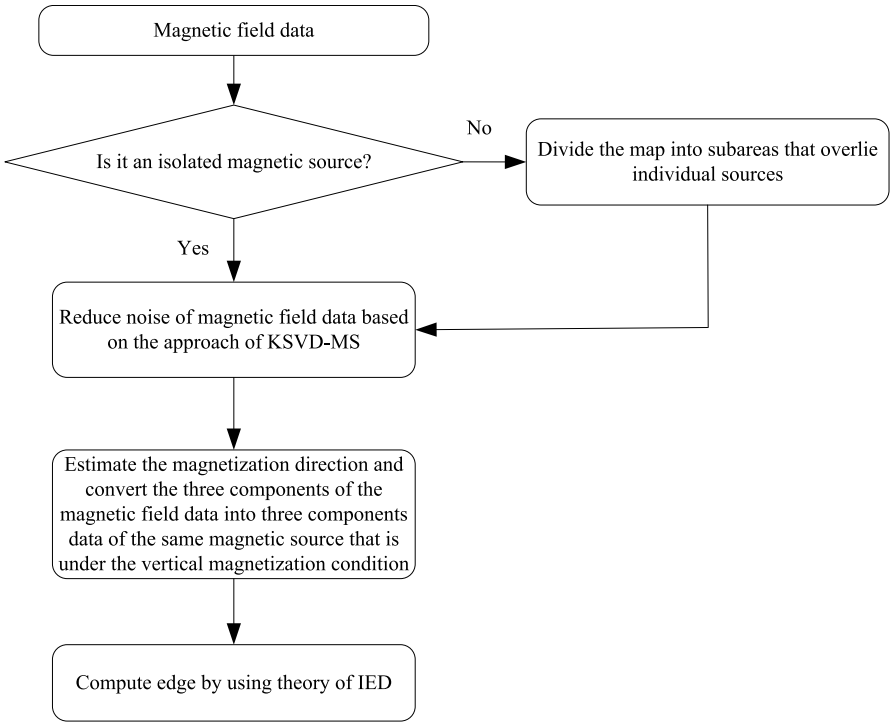

FIGURE 3. Flow chart of edge detection method.

and the B_{zz} component data under the vertical magnetization condition to calculate the edges of the magnetic sources. The IED calculation formula can be expressed as:

$$\text{IED} = \arctan\left[\frac{I}{B_{zz}}\right] \tag{13}$$

Under the vertical magnetization condition, the magnetic gradient tensor B_{zz} component contains positive and negative values, and the intersection of positive and negative data corresponds to the edges of the magnetic sources. Therefore, the zero contour of the IED corresponds to the edges of the magnetic sources.

D. CALCULATION PROCEDURES

Based on the above analysis, we can calculate the edges of magnetic sources through the magnetic gradient tensor with the oblique magnetization direction. The calculation processes are shown as follows (see Fig. 3 for a flow chart):

1. The number of magnetic sources is determined based on the main positive value of the NSS data. Then, if the calculation area includes multiple magnetic sources, the calculation area would need to be divided. The observation surface is divided into subareas that contain isolated magnetic source;
2. The denoised magnetic field data is calculated by using the KSVD-MS;
3. The magnetization direction is estimated according to (9). Based on it, (10) and (11) are used to convert the three components of the magnetic field data into the data of three components from the same magnetic source under the vertical magnetization condition;
4. The IED is calculated by using (13) to obtain edges of magnetic sources.

III. DATA EXPERIMENTS

A. TEST ON SYNTHETIC MAGNETIC DATA

1) ISOLATED MODEL

First of all, an isolated rectangular prism under the oblique magnetization condition was used to prove the effectiveness of the method proposed in this paper. The length of the rectangular prism in the N-S direction is 1.4 m, the length in the E-W direction is 1.4 m, and the length in the vertical direction is 0.2 m. The center of the rectangular prism is (2.2m, 2.2m, 0.6m). This model has an inclination of 40°, a declination of 15°, and a magnetic intensity of 30 A/m. It is assumed that the height of the observation surface is 0m, the spacing of the observation points is 0.1m, and the observation surface is a grid of 42 × 42. The baseline distance in the simulation is 0.1m, and the magnetic data detection system is shown in Fig. 1. In the actual process of measurement, the edge detection result of the magnetic source would be affected by the noise contained in the measured magnetic data. Therefore, the white Gaussian noise with 30 dB was added to the magnetic field data generated by rectangular prism at each point in order to simulate the actual measurement situation. The model has an estimated inclination of 37° and an estimated declination of 14°. In this study, the estimated magnetization direction was used to convert the three components

TABLE 1. Method 1 is Low-pass filter, method 2 is wavelet soft threshold filter, method 3 is EMD, method 4 is KSVD, method 5 is KSVD-MS.

Method	SNR						RMSE					
	B_{xx}	B_{xy}	B_{xz}	B_{yy}	B_{yz}	B_{zz}	B_{xx}	B_{xy}	B_{xz}	B_{yy}	B_{yz}	B_{zz}
1	45.40	29.36	41.07	27.11	26.12	36.49	473.83	481.05	630.47	859.28	1006.99	1034.23
2	62.18	46.19	58.78	49.57	59.02	59.71	212.04	243.67	285.56	313.33	233.38	345.67
3	35.57	32.90	26.27	11.02	29.42	22.22	807.43	467.57	1472.26	2051.18	983.64	2176.63
4	35.28	50.72	25.81	38.65	44.30	40.84	829.13	192.78	1528.05	524.12	478.45	882.81
5	68.07	54.03	63.89	65.89	61.93	70.42	158.05	164.27	221.45	137.39	200.93	201.83

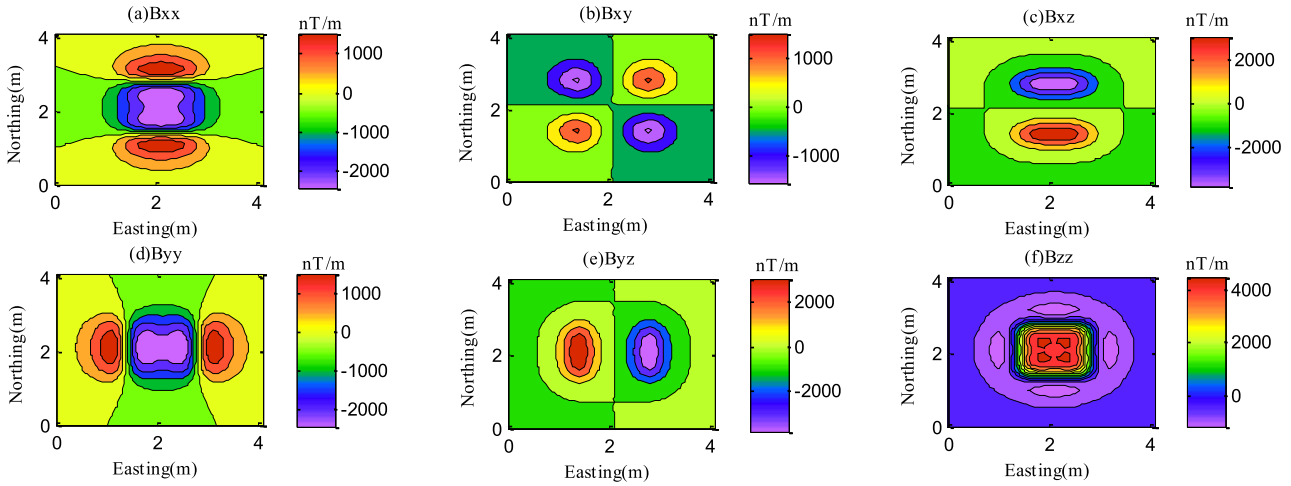

FIGURE 4. The theoretical magnetic gradient tensor maps of the rectangular prism under the vertical magnetization condition. (a), (b), (c), (d), (e) and (f) represent B_{xx}, B_{xy}, B_{xz}, B_{yy}, B_{yz} and B_{zz} component, respectively.

of the magnetic field data into three components data of the same magnetic source under the vertical magnetization condition. Then, the magnetic gradient tensor of the same magnetic source under the vertical magnetization condition could be acquired. Besides, the comparison of the results obtained from Low-pass filter, wavelet soft threshold, Empirical Mode Decomposition (*EMD),* and KSVD was performed to illustrate the effectiveness of the proposed method; the denoised results were shown in Table 1. The signal-to-noise (SNR) and root-mean-squared-error (RMSE) were used as evaluation indicators to judge the denoised ability ($\mathrm{SNR} = 10\lg\left\{\sum_{i=1}^{M}\sum_{j=1}^{N}T(i,j)^2\Big/\sum_{i=1}^{M}\sum_{j=1}^{N}(T(i,j)-\overline{T}(i,j))\right\}$ and $\mathrm{RMSE} = \sum_{i=1}^{M}\sum_{j=1}^{N}(T(i,j)-\overline{T}(i,j))^2\Big/M\cdot N$). Parameters ($v = 10$, $l = 1$) and calculation results obtained by different denoised methods are shown in Table 1. It can be found from Table 1, that the KSVD-MS has the best denoised effect.

The theoretical magnetic gradient tensor components of the rectangular prism under the vertical magnetization condition are shown in Fig. 4 in order to explain the effectiveness of the proposed method. Noisy magnetic gradient tensor components of the rectangular prism under the oblique magnetization condition are shown in Fig. 5 (*a*), (*b*), (*c*), (*g*), (*h*), and (*i*). The denoised components of B_{xx}, B_{xy}, B_{xz}, B_{yy}, B_{yz}, and B_{zz} obtained under the vertical magnetization condition using the proposed method are shown in Fig. 5 (*d*), (*e*), (*f*), (*j*), (*k*), and (*l*). According to Figs. 4 and 5, the KSVD-MS has a great ability to reduce noise. Besides, the magnetic gradient tensor components can be effectively converted into the data from the same magnetic source by the proposed method under the vertical magnetization condition. Under the vertical magnetization condition, the THD map, the Theta map, the Tilt angle map, and the IED map are shown in Fig. 6. It can be seen that the IED method is more effective than other methods under the vertical magnetization condition. The THD, Theta, Tilt angle, and IED maps obtained by using noisy magnetic gradient tensor components of the rectangular prism under the oblique magnetization condition are displayed in Fig. 7 (*a*), (*b*), (*c*) and (d); the IED map obtained by using the preprocessed method in this paper is shown in Fig. 7 (*e*) and (*f*). As shown in Fig. 7, calculation

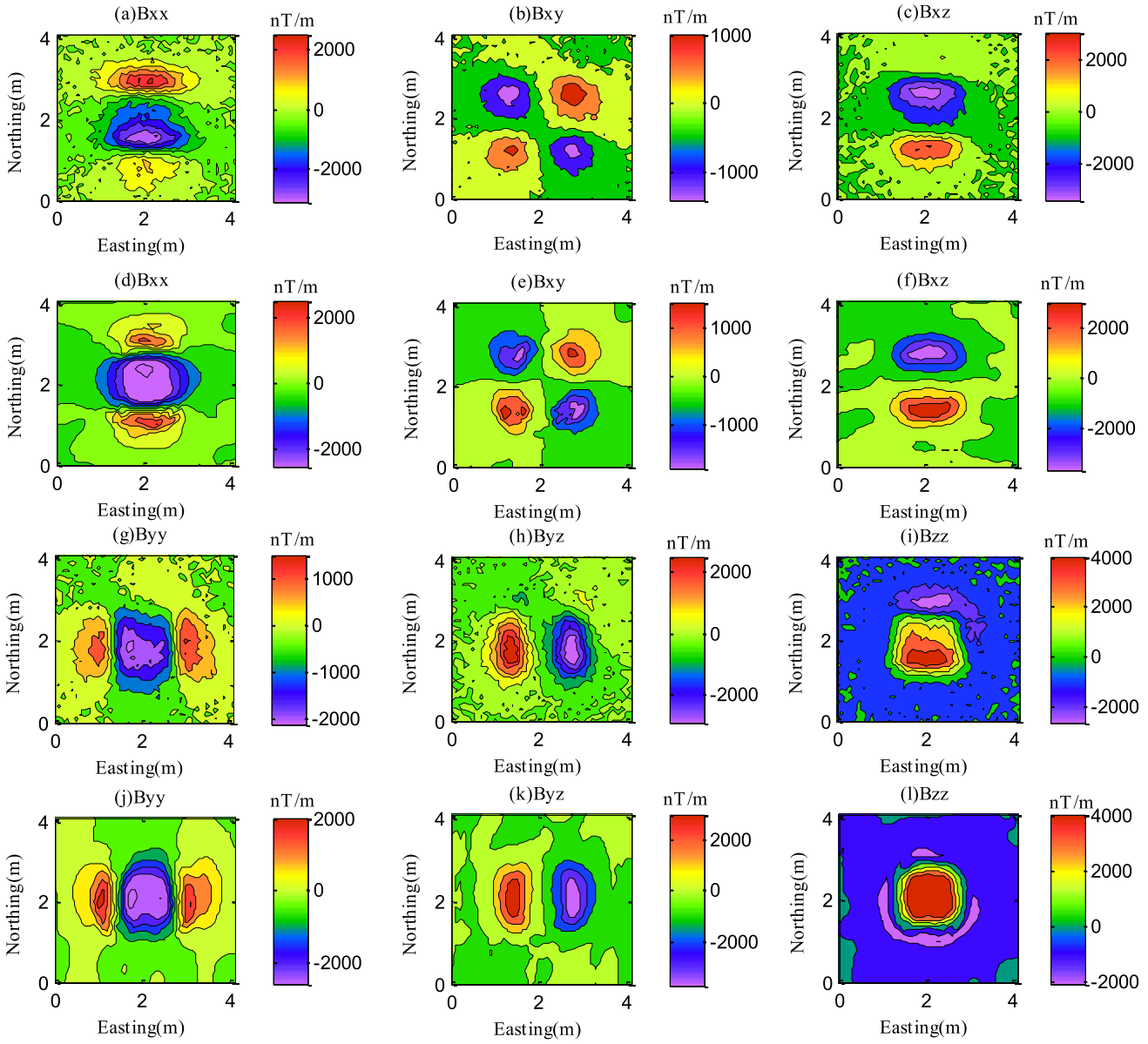

FIGURE 5. Magnetic gradient tensor maps after noise is added to the data in Fig. 4 and the denoised magnetic gradient tensor maps by using the proposed method. (a), (b), (c), (g), (h) and (i) represent B_{xx}, B_{xy}, B_{xz}, B_{yy}, B_{yz} and B_{zz} component with noise, respectively. And (d), (e), (f), (j), (k) and (l) represent the denoised B_{xx}, B_{xy}, B_{xz}, B_{yy}, B_{yz} and B_{zz} component, respectively.

TABLE 2. The physical parameters of the four rectangular prisms.

model	Center coordinates (m)	Thickness (m)	Length in the N-S direction (m)	Length in the E-W direction (m)
1	(2.8,0.9,0.525)	0.95	1.6	0.5
2	(1.3,2.9,0.6)	0.8	1.6	0.5
3	(0.7,1.1,0.575)	0.85	0.5	0.8
4	(3.3,2.9,0.55)	0.9	0.5	0.8

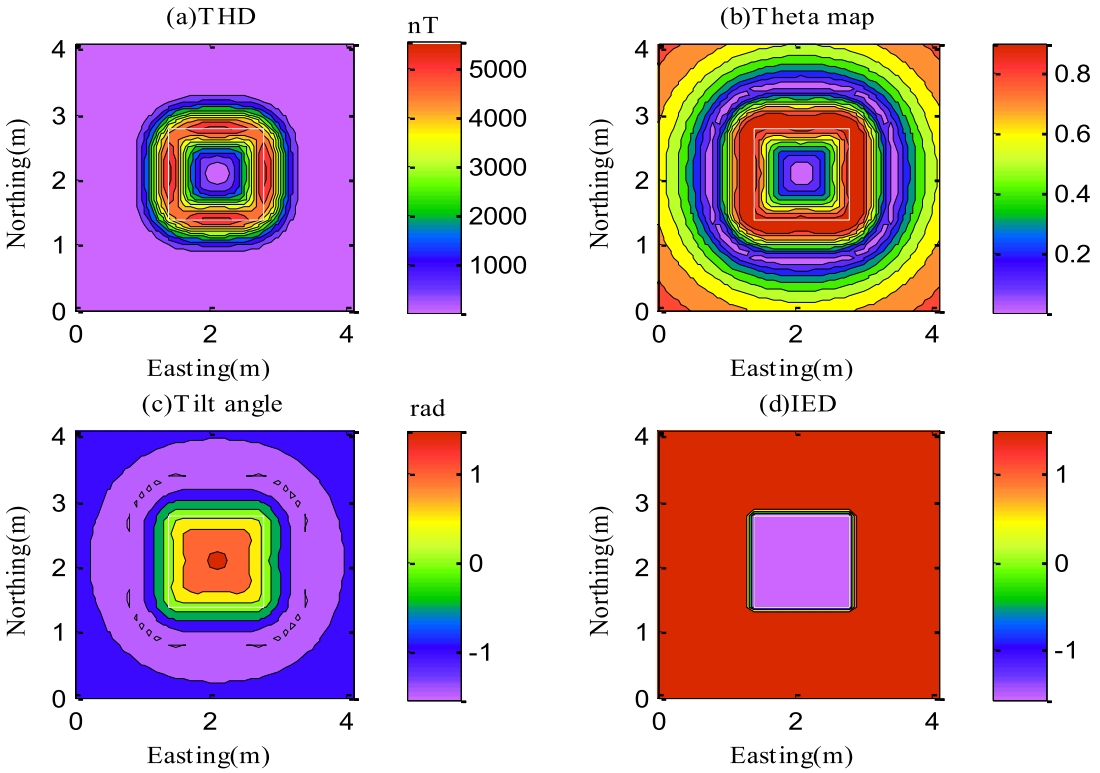

FIGURE 6. The theoretical edge detection results of different methods under the vertical magnetization condition. (a), (b), (c) and (d) represent the THD map, the Theta map, the Tilt map angle and the IED map.

TABLE 3. The results of esitmated magnetization direction for the four models. E is the difference between the theoretical value and the estimated value. $\theta = \arccos(\alpha_1\alpha_2 + \beta_1\beta_2 + \gamma_1\gamma_2)$ is the difference between the actual magnetization directions and the estimated magnetization directions.

model	Model parameters (deg)		Parameters estimated (deg)		
	inclination	declination	inclination (E)	declination (E)	θ
1	50	50	54(4)	62(12)	8.39
2	60	60	65(5)	52(-8)	6.21
3	40	-30	42(2)	-24(6)	4.95
4	20	-10	20(0)	-9(1)	0.94

results of all the methods are damaged under the influence of noise and oblique magnetization. Moreover, Theta and Tilt angle maps have more noise compared to THD and IED maps. It can be seen from Fig. 7 (e) and (f) that the best effect of edge detection can be obtained by using the proposed method of this paper. The edge of the rectangular prism has a large error between the calculated position and theoretical position when the calculation method is not performed. This comparison verifies that the method of this paper has excellent noise resistance and can accurately obtain the edge of magnetic source under the oblique magnetization condition.

2) MULTIPLE MODELS

Next, a combination of four rectangular prisms was used in this paper for the simulation in order to verify the effectiveness of the proposed method for multiple magnetic sources. The physical parameters of the four rectangular prisms are shown in Table 2. The magnetic gradient tensor, NSS, and TMI generated by four rectangular prisms with 30 dB white

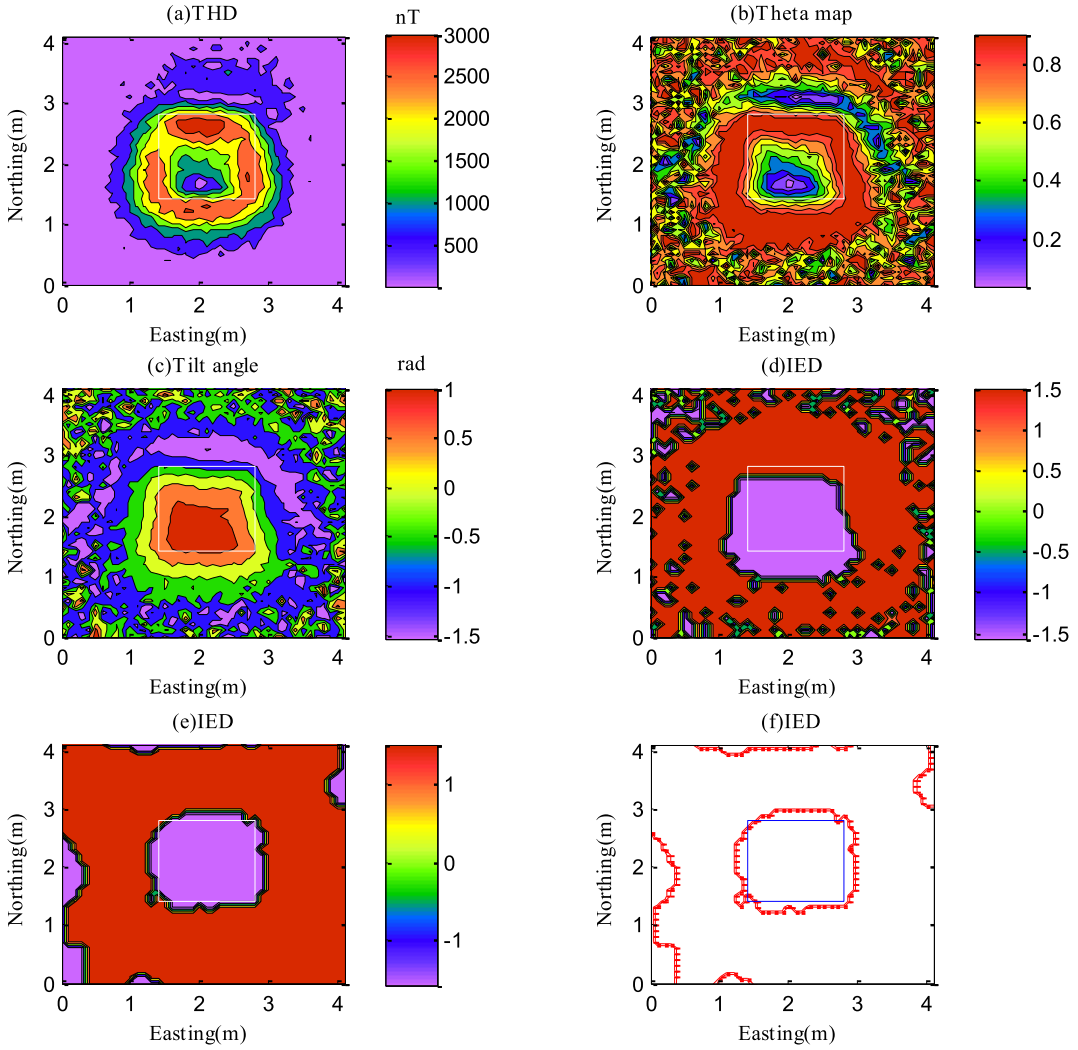

FIGURE 7. The noisy edge detection results of different methods under the oblique magnetization condition. (a), (b), (c) and (d) represent the THD map, the Theta map, the Tilt map angle and the IED map without using the preprocessed method in this paper. (e) and (f) represent the IED map and the zero-contour of the IED map by using the preprocessed method in this paper. The solid line is consistent with the actual position of the magnetic source.

Gaussian noise are shown in Fig. 8. It is assumed that the height of the observation surface is 0m, the spacing of the observation points is 0.1m, and the observation surface is a grid of 42 × 42. The position of the main positive value on the NSS map coincides with the actual position of the magnetic sources, indicating that the NSS can provide the effective position information of the magnetic sources under the oblique magnetization condition. In this paper, subareas that overlie individual sources were selected according to the calculated NSS map. Besides, multiple magnetic sources were separated by dividing different isolated subareas. T[he SNR of the NSS data can be improved; the accuracy of edge detection can be improved.

Original magnetic gradient tensor B_{xx}, B_{xy}, B_{xz}, B_{yy}, B_{yz}, and B_{zz} data are shown in Fig. 8; the denoised magnetic gradient tensor components obtained by using KSVD-MS is shown in Fig. 9. It can be found from Fig. 9 that the SNR of the magnetic gradient tensor can be effectively improved by the KSVD-MS method. According to Table 3, the estimation results of the magnetization direction have a good agreement with the theoretical values. The difference between actual magnetization directions and estimated magnetization directions are about $6° - 8°$. The magnetic gradient tensor component B_{zz} was converted into the B_{zz} from the same magnetic source under the vertical magnetization condition by using the estimated magnetization directions. B_{zz}maps of the magnetic sources in Fig. 8(f) obtained by using the preprocessed method in this paper are shown in Fig. 10 (e)- (h). The solid line is consistent with the actual position of magnetic sources. Comparing the unconverted B_{zz} data in the calculation windows (Fig. 10 (a)-(d)) with the converted B_{zz} data (Fig. 10 (e)-(h)), it can be seen that the B_{zz} data obtained using the preprocessed method in this paper can better represent the contour of the model, further verifying

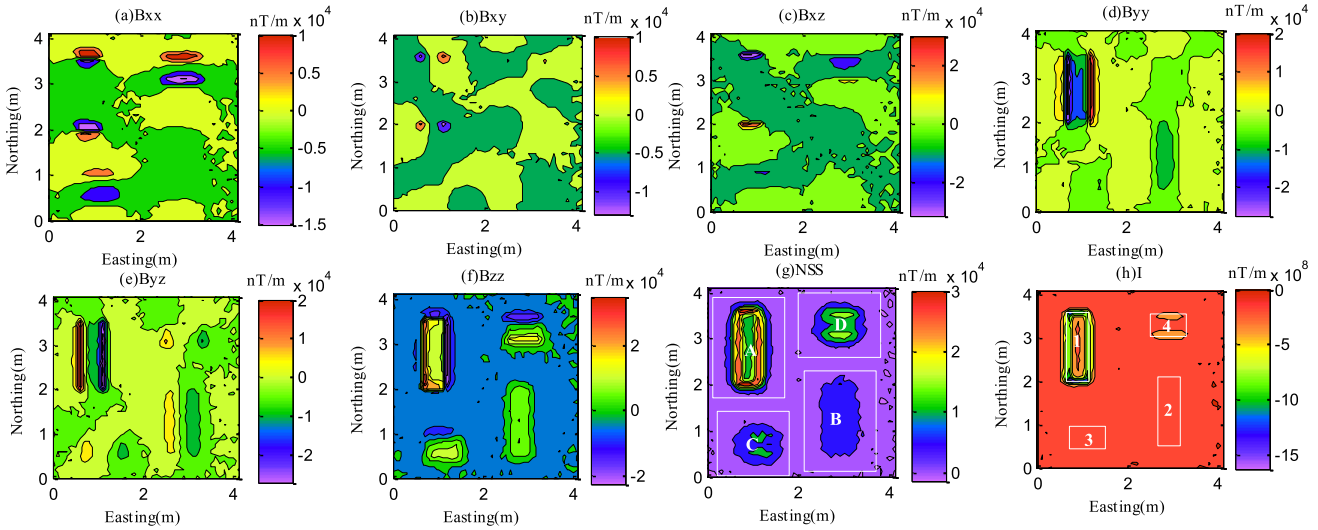

FIGURE 8. Magnetic gradient tensor, NSS and I maps of the four rectangular prisms with noise. (a), (b), (c), (d), (e), (f), (g) and (h) represent B_{xx}, B_{xy}, B_{xz}, B_{yy}, B_{yz}, B_{zz}, NSS and I, respectively. The solid line is consistent with the actual position of the magnetic sources.

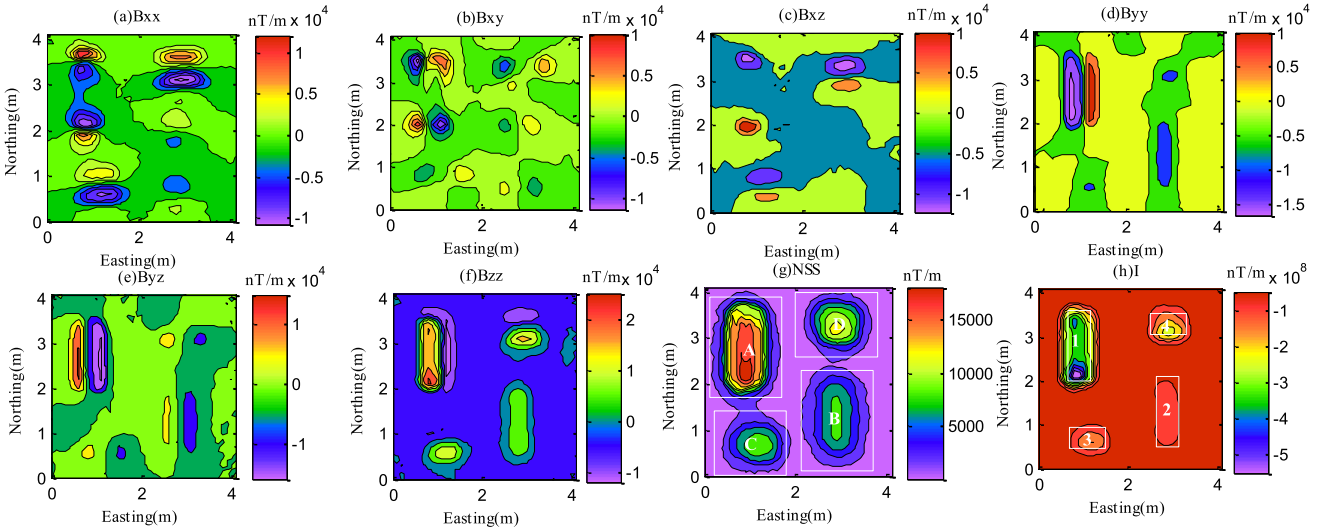

FIGURE 9. The denoised magnetic gradient tensor, NSS and I maps of the four rectangular prisms by using KSVD-MS method. (a), (b), (c), (d), (e), (f), (g) and (h) represent B_{xx}, B_{xy}, B_{xz}, B_{yy}, B_{yz}, B_{zz}, NSS and I, respectively. The solid line is consistent with the actual position of the magnetic sources.

TABLE 4. The results of esitmated magnetization direction for the two models. $\theta = \arccos(\alpha_1\alpha_2 + \beta_1\beta_2 + \gamma_1\gamma_2)$ is the difference between the actual magnetization directions and the estimated magnetization directions.

Source	Model parameters (deg)		Parameters estimated (deg)		
	inclination	declination	inclination	declination	θ
1	57	-16	12	-5	44.97
2	57	-16	3	-13	53.08

that the magnetization direction of the magnetic source can be well-estimated by the preprocessed method in this paper.

The calculated maps of edge detection without using the preprocessed method are illustrated in Fig. 11 (*a*)-(*d*). Edge detection results obtained by the THD method, the Theta map

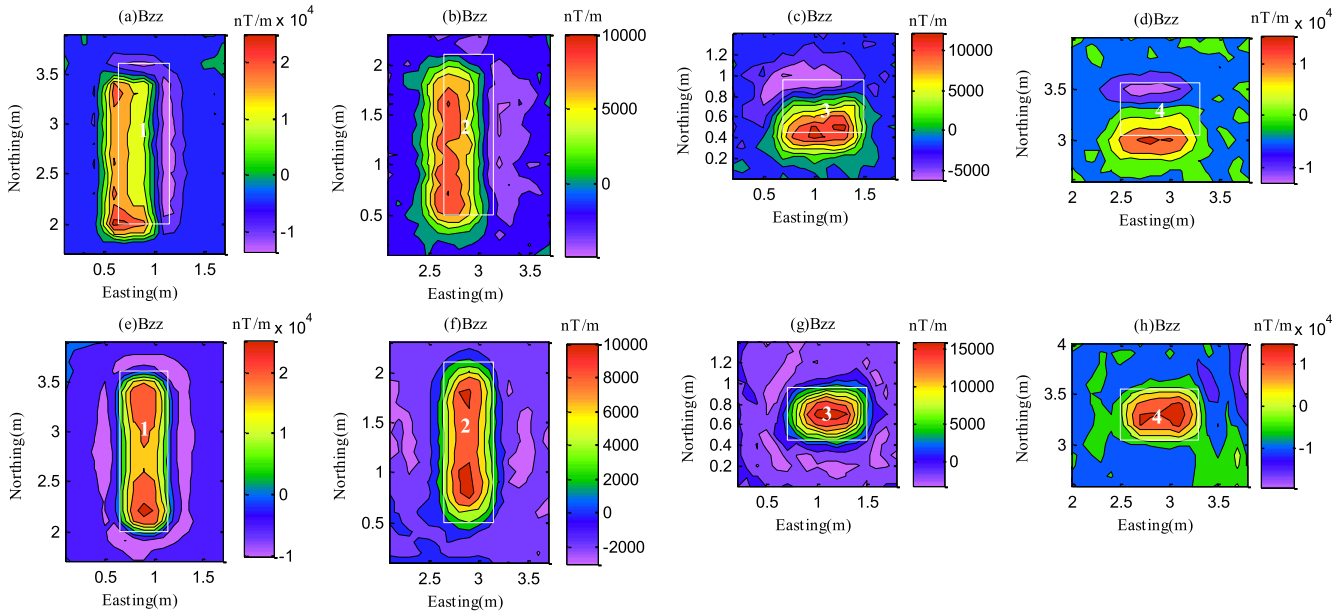

FIGURE 10. (a), (b), (c) and (d) represent B_{zz} maps of the Window A, B, C and D in Fig. 8(g), respectively, without using the preprocessed method in this paper. (e), (f), (g) and (h) represent B_{zz} maps of the Window A, B, C and D in Fig. 8(g), respectively, with using the preprocessed method in this paper.

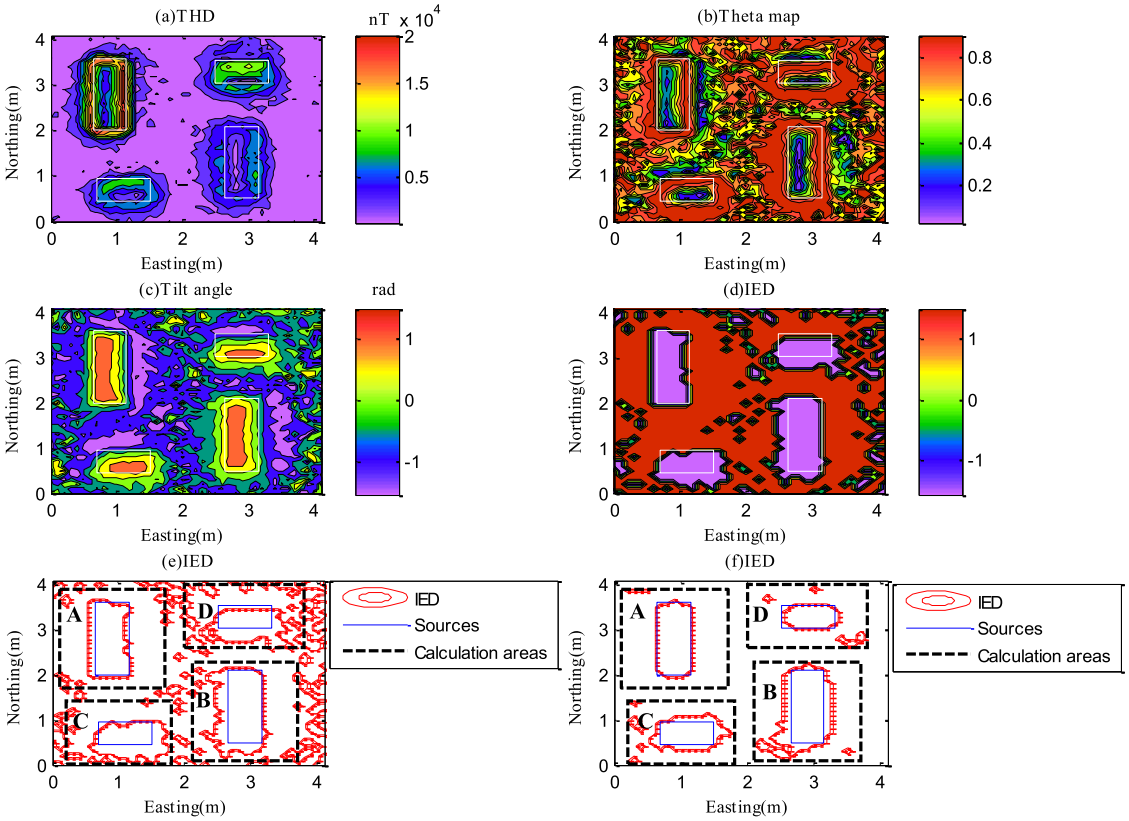

FIGURE 11. The noisy edge detection results of different methods under the oblique magnetization condition. (a), (b), (c) and (d) represent the THD map, the Theta map, the Tilt map angle and the IED map without using the preprocessed method in this paper. (e) and (f) represent the zero-contour of the IED maps without and with using the preprocessed method in this paper, respectively. The solid line is consistent with the actual position of the magnetic source and the dotted line represents the calculation areas.

TABLE 5. Method 1 is Low-pass filter, method 2 is wavelet soft threshold filter, method 3 is EMD, method 4 is KSVD, method 5 is KSVD-MS.

Method	SNR						RMSE(10^3)					
	B_{xx}	B_{xy}	B_{xz}	B_{yy}	B_{yz}	B_{zz}	B_{xx}	B_{xy}	B_{xz}	B_{yy}	B_{yz}	B_{zz}
1	13.88	13.41	11.53	11.79	7.03	14.47	5.98	4.88	7.36	5.03	7.71	9.47
2	48.48	33.65	49.42	34.52	57.57	49.31	1.38	1.81	1.56	1.78	0.93	2.03
3	19.27	11.28	11.12	15.97	12.94	22.61	6.62	5.92	7.78	4.54	6.46	7.95
4	45.48	50.11	53.42	49.18	56.69	52.81	1.54	0.82	1.22	0.88	0.95	1.66
5	51.30	51.49	57.39	49.41	58.27	57.98	1.14	0.81	1.02	0.90	0.87	1.28

FIGURE 12. The magnetic gradient tensor system.

method, and the Tilt angle method have a large deviation from the actual edge of magnetic sources and are sensitive to noise. According to Fig. 11 (a)-(d), the IED method can obtain a sharper edge of a magnetic source; however, the edge obtained still deviates from the actual edge when we did not use the preprocessed method. It can be seen from the comparison of IED maps of Fig. 11 (*e*) and (*f*) that the horizontal edge position of the IED method obtained by using the preprocessed method has better consistency with the horizontal position of actual magnetic sources. Thus, the method of this paper has a better edge detection ability for multiple models under oblique magnetization and noise conditions.

B. TEST ON THE REAL MAGNETIC DATA

The actual measurement experiment was performed in Shijiazhuang, China. Two rectangular prisms were placed in the measurement area. The spacing of the observation points was 0.1 m; the observation surface was a grid of 2.1m × 1.9m; the geomagnetic inclination was 55°; the geomagnetic declination was −16°. The magnetic gradient tensor system

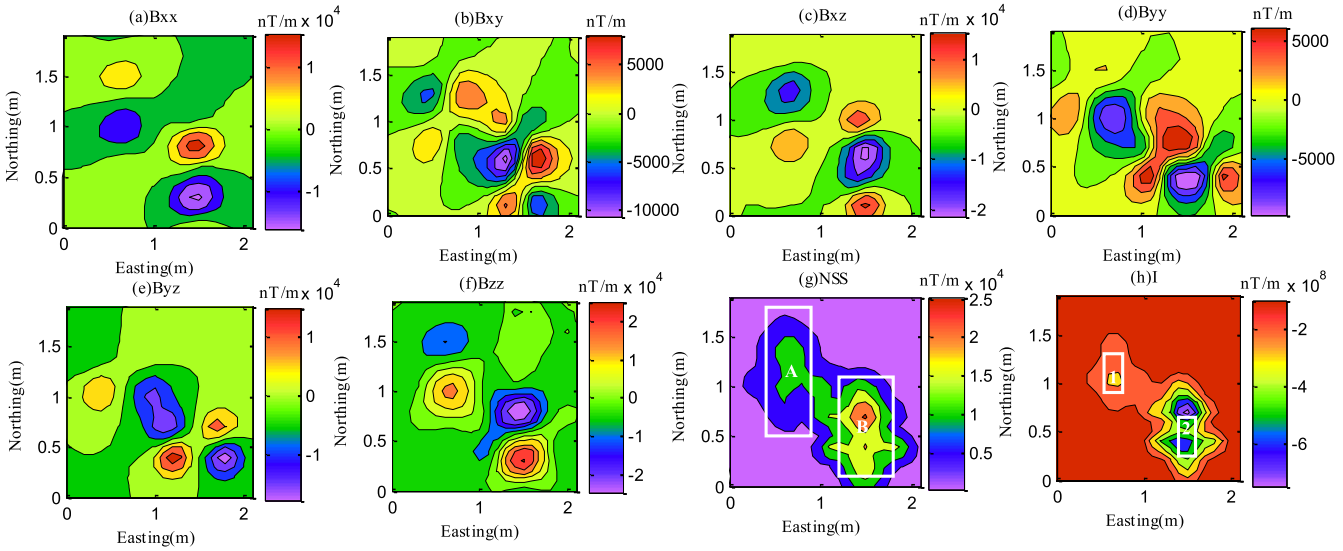

FIGURE 13. The original magnetic gradient tensor, NSS and I maps of the two rectangular prisms. (a), (b), (c), (d), (e), (f), (g) and (h) represent B_{xx}, B_{xy}, B_{xz}, B_{yy}, B_{yz}, B_{zz}, NSS and I, respectively. The solid line is consistent with the actual position of the two rectangular prisms.

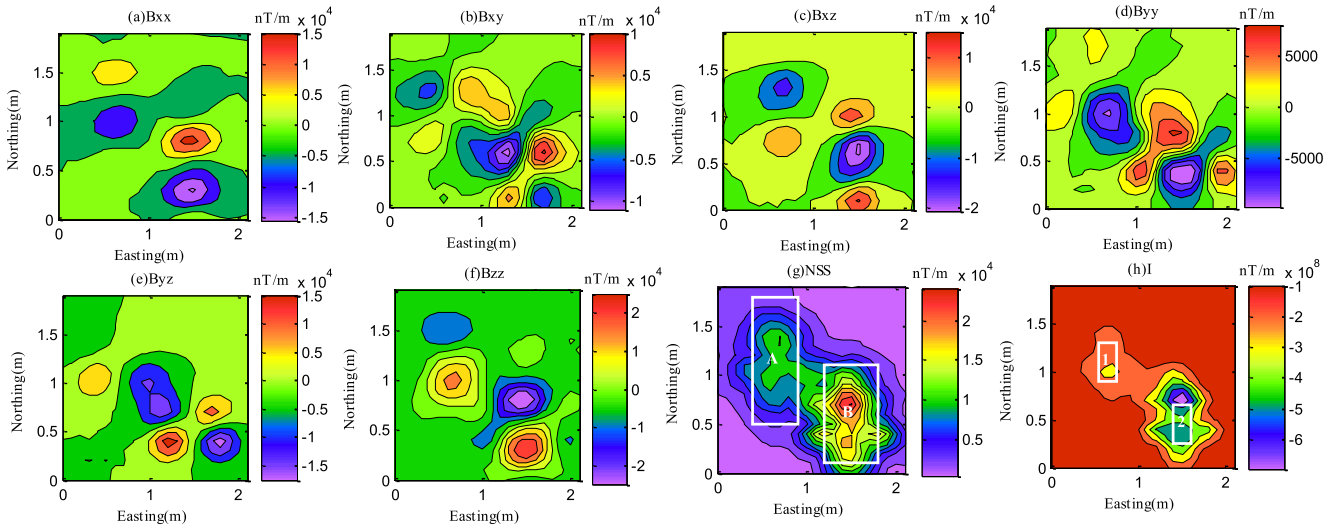

FIGURE 14. The denoised magnetic gradient tensor, NSS and I maps of the two rectangular prisms by using KSVD-MS method. (a), (b), (c), (d), (e), (f), (g) and (h) represent B_{xx}, B_{xy}, B_{xz}, B_{yy}, B_{yz}, B_{zz}, NSS and I, respectively. The solid line is consistent with the actual position of the two rectangular prisms.

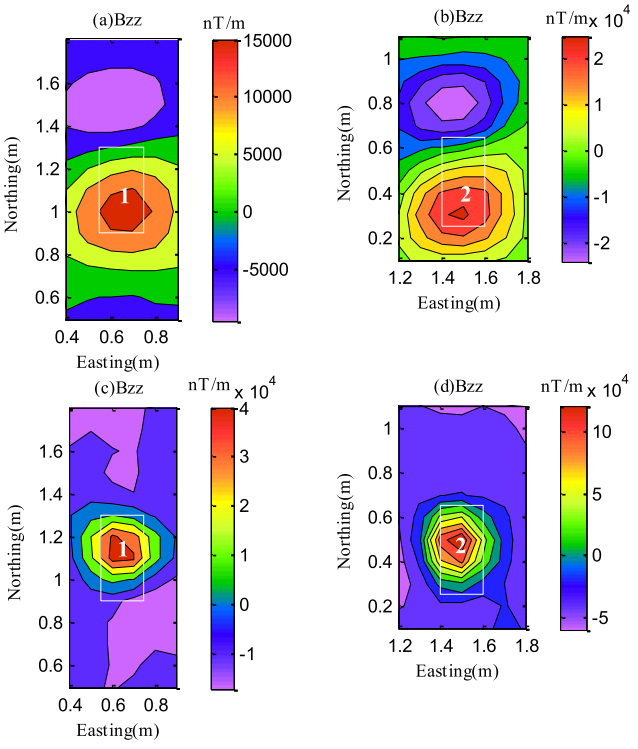

FIGURE 15. (a) and (b) represent B_{zz} maps of the Window A and B in Fig. 13(g), respectively, without using the preprocessed method in this paper. (c) and (d) represent B_{zz} maps of the Window A and B in Fig. 13(g), respectively, with using the preprocessed method in this paper.

used in the experiment is shown in Fig. 12. The system consisted of four mag-03 tri-axial fluxgate magnetometers and a cross-type plastic bracket. The baseline distance between the two magnetometers was 0.4 m. The nonorthogonality error of the sensor and the misalignment error between the sensors are corrected by nonlinear least squares [24]. Besides, the measured magnetic gradient tensor, NSS data, and magnetic gradient tensor invariant are shown in Fig. 13. The sizes of the rectangular prism labeled 1 in Fig. 13(*h*) were N-S length = 0.36 m and E-W width = 0.23 m with the center of (1.15 m, 0.65 m). The top depth was 0.2 m and the depth extent was 0.1 m. The sizes of the rectangular prism labeled 2 in Fig. 13(*h*) were N-S length = 0.36m and E-W width = 0.234 m with the center of (0.45 m, 1.5 m). The top depth was 0.15 m and the depth extent was 0.05 m. In this study, the subareas that overlie individual sources were selected according to the calculated NSS map; besides, the multiple magnetic sources were separated by dividing different isolated subareas, as shown in Fig. 13 (*g*). Moreover, the denoised magnetic gradient tensor obtained by using KSVD-MS is shown in Fig. 14. Calculation results obtained by different denoised methods are shown in Table 5. It can be seen from Table 5 that the denoised method proposed in this paper has the best denoising effect. The estimation results of the magnetization direction are shown in Table 4. In this study, the magnetic gradient tensor component B_{zz} (Fig. 15(a) and (b)) were converted into the B_{zz} (Fig. 15(c) and (d)) from the same magnetic sources under the vertical magnetization condition by using estimated magnetization directions. The difference between the geomagnetic magnetization direction and estimated magnetization directions of magnetic sources 1 and 2 in Table 4 are 44.97° and 53.08°, respectively.

The calculated maps of edge detection without using the preprocessed method are displayed in Fig. 16 (*a*)-(*d*). Edge detection results obtained by the THD method, the Theta map method, and the Tilt angle method have a large deviation from the actual edges of magnetic sources. By comparing IED maps of Fig. 16 (*e*) and (*f*), it can be seen that the horizontal edge position of the IED method acquired by using the preprocessed method has better consistency with the horizontal position of actual magnetic sources; this result is consistent with the discussion of the simulation chapter.

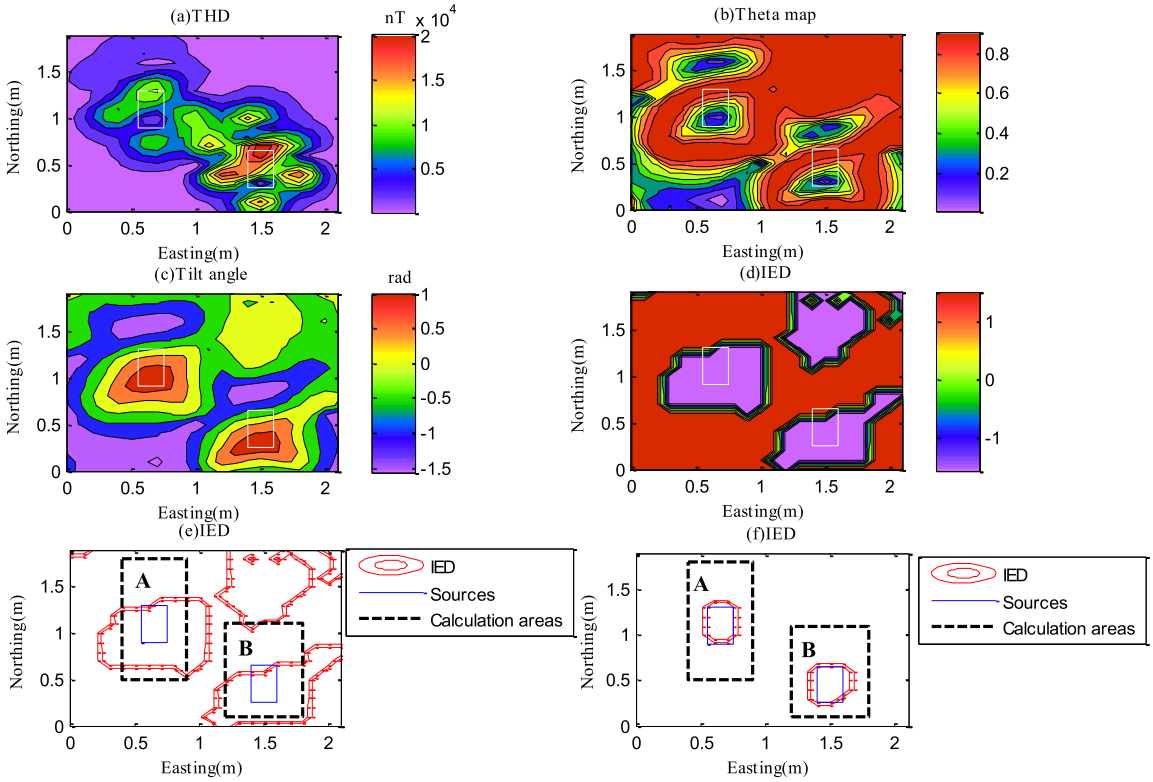

FIGURE 16. The edge detection results of different methods. (a), (b), (c) and (d) represent the THD map, the Theta map, the Tilt map angle and the IED map without using the preprocessed method in this paper. (e) and (f) represent the zero-contour of the IED maps without and with using the preprocessed method in this paper, respectively. The solid line is consistent with the actual position of the magnetic source and the dotted line represents the calculation areas.

Therefore, the edges of magnetic sources under the oblique magnetization condition can be effectively reconstructed by the method proposed in this paper; moreover, this method has an excellent ability to reduce noise.

In experimental results, there are some errors between calculation results and the actual position. In the actual experimental process, the observed data is affected not only by the system's own error but also by the operator. In the future, the magnetic gradient tensor system will be further improved; the experimental operation will be standardized in order to improve the accuracy of measured magnetic data.

IV. CONCLUSIONS

In this paper, a new edge detection method of magnetic sources under the oblique magnetization condition has been proposed. According to the inter-relationship between different magnetic field components, the magnetic field components are transformed into total magnitude anomaly and its direction cosines; then, the IKSVD-MS method is used to reconstruct the magnetic signal. Besides, a correlation coefficient analysis is performed to calculate the actual magnetization direction of magnetic anomalies. Next, the magnetic gradient tensor data is converted into the data from the same magnetic source under the vertical magnetization condition. The edge of the magnetic source is calculated through the ratio of the magnetic gradient tensor invariant to the B_{zz} component data under the vertical magnetization condition. Finally, the method proposed in this paper is tested and verified by simulation and experiment. The obtained simulation and experimental results show that the effects of oblique magnetization can be considerably reduced by this method. Furthermore, the method in this paper has good resistance to noise.

REFERENCES

[1] H. G. Miller and V. Singh, "Potential field tilt—A new concept for location of potential field sources," *J. Appl. Geophys.*, vol. 32, nos. 2–3, pp. 213–217, Aug. 1994, doi: 10.1016/0926-9851(94)90022-1.

[2] G. Q. Ma, "Combination of horizontal gradient ratio and Euler methods for the interpretation of potential field data," *Geophysics*, vol. 78, no. 5, pp. J53–J60, Sep. 2013, doi: 10.1190/geo2012-0490.1.

[3] B. Verduzco, J. D. Fairhead, C. M. Green, and C. MacKenzie, "New insights into magnetic derivatives for structural mapping," *Lead. Edge*, vol. 23, no. 2, pp. 116–119, Feb. 2004, doi: 10.1190/1.1651454.

[4] C. Wijns, C. Perez, and P. Kowalczyk, "Theta map: Edge detection in magnetic data," *Geophysics*, vol. 70, no. 4, pp. L39–L43, Jul. 2005, doi: 10.1190/1.1988184.

[5] G. Ma and L. Li, "Edge detection in potential fields with the normalized total horizontal derivative," *Comput. Geosci.*, vol. 41, pp. 83–87, Apr. 2012, doi: 10.1016/j.cageo.2011.08.016.

[6] L. Li, G. Ma, and X. Du, "Edge detection in potential-field data by enhanced mathematical morphology filter," *Pure Appl. Geophys.*, vol. 170, no. 4, pp. 645–653, Apr. 2013, 10.1007/s00024-012-0545-x.

[7] W. Du, Y. Wu, Y. Guan, and M. Hao, "Edge detection in potential filed using the correlation coefficients between the average and standard deviation of vertical derivatives," *J. Appl. Geophys.*, vol. 143, pp. 231–238, Aug. 2017, doi: 10.1016/j.jappgeo.2017.01.002.

[8] M. N. Nabighian, "The analytic signal of two-dimensional magnetic bodies with polygonal cross-section: Its properties and use for automated anomaly interpretation," *Geophysics*, vol. 37, pp. 507–517, Jun. 1972, doi: 10.1190/1.1440276.
[9] W. R. Roest, J. Verhoef, and M. Pilkington, "Magnetic interpretation using the 3-D analytic signal," *Geophysics*, vol. 57, pp. 116–125, Jan. 1992, doi: 10.1190/1.1443174.
[10] S. Qin, "An analytic signal approach to the interpretation of total field magnetic anomalies," *Geophys. Prospecting*, vol. 42, pp. 665–675, Apr. 1994, doi: 10.1111/j.1365-2478.1994.tb00234.x.
[11] Z. N. Guan and C. L. Yao, "Inversion of the total gradient modulus of magnetic anomaly due to dipping dike," *Earth Sci., J. China Univ. Geosci.*, vol. 22, pp. 81–85, Jan. 1997.
[12] X. Li, "Understanding 3D analytic signal amplitude," *Geophysics*, vol. 71, pp. L13–L16, Mar. 2006, doi: 10.1190/1.2184367.
[13] M. Beiki, D. A. Clark, J. R. Austin, and C. Foss, "Estimating source location using normalized magnetic source strength calculated from magnetic gradient tensor data," *Geophysics*, vol. 77, pp. J23–J37, Nov. 2012, doi: 10.1190/geo2011-0437.1.
[14] Y. Gang, Z. Yingtang, F. Hongbo, L. Zhining, and R. Guoquan, "Detection, localization and classification of multiple dipole-like magnetic sources using magnetic gradient tensor data," *J. Appl. Geophys.*, vol. 128, pp. 131–139, May 2016, doi: 10.1016/j.jappgeo.2016.03.022.
[15] M. Pilkington and M. Beiki, "Mitigating remanent magnetization effects in magnetic data using the normalized source strength," *Geophysics*, vol. 78, pp. J25–J32, Apr. 2013. 10.1190/geo2012-0225.1.
[16] H. Yu, "Geomagnetic field measurement and study on underwater magnetic localization technology," Ph.D. dissertation, College Automat., Harbin Eng. Univ., Harbin, China, 2011.
[17] M. Elad and M. Aharon, "Image denoising via sparse and redundant representations over learned dictionaries," *IEEE Trans. Image Process.*, vol. 15, no. 12, pp. 3736–3745, Dec. 2006, doi: 10.1109/TIP.2006.881969.
[18] D. Needell and R. Vershynin, "Signal recovery from incomplete and inaccurate measurements via regularized orthogonal matching pursuit," *IEEE J. Sel. Topics Signal Process.*, vol. 4, no. 2, pp. 310–316, Apr. 2010.
[19] A. P. Richard, "A new algorithm for image noise reduction using mathematical morphology," *IEEE Trans Image Process.*, vol. 4, no. 3, pp. 542–548, May 1995, doi: 10.1109/83.382491.
[20] H. Chen, C. Wang, X. Zuo, and H. Zhu, "Metal magnetic memory gradient tensor signal processing method," *Syst. Eng. Electron.*, vol. 39, no. 3, pp. 488–493, Mar. 2017, doi: 10.3969/j.issn.1001-506X.2017.03.05.
[21] J. Li, Y. Zhang, G. Yin, H. Fan, and Z. Li, "An approach for estimating the magnetization direction of magnetic anomalies," *J. Appl. Geophys.*, vol. 137, pp. 1–7, Feb. 2017, doi: 10.1016/j.jappgeo.2016.12.009.
[22] G. Yin, Y. Zhang, S. Mi, H. Fan, and Z. Li, "Calculation of the magnetic gradient tensor from total magnetic anomaly field based on regularized method in frequency domain," *J. Appl. Geophys.*, vol. 134, pp. 44–54, Nov. 2016, doi: 10.1016/j.jappgeo.2016.08.010.
[23] J. Li, Y. Zhang, H. Fan, and M. Liu, "Estimating the location of magnetic sources using magnetic gradient tensor data," *Explor. Geophys.*, vol. 50, no. 6, pp. 600–612, May 2019, doi: 10.1080/08123985.2019.1615834.
[24] Q. Li, Z. Li, Y. Zhang, and G. Yin, "Artificial vector calibration method for differencing magnetic gradient tensor systems," *Sensors*, vol. 18, p. 361, Jan. 2018, doi: 10.3390/s18020361.

JINPENG LI was born in Changchun, China, in 1991. He received the B.S. degree in vehicle engineering from the University of Jilin, Changchun, China, in 2014, and the M.S. degree in mechanical engineering from the Ordnance Engineering College, Shijiazhuang, China, in 2017. He is currently pursuing the Ph.D. degree in mechanical engineering with Army Engineering University, Shijiazhuang.

Since 2017, he has been a student of the Seventh Department, Army Engineering University, Shijiazhuang, China. His research interests include sensor testing technology and signal processing.

Mr. Li received the Excellent Master Thesis of Ordnance Engineering College.

YINGTANG ZHANG was born in Shijiazhuang, China, in 1960. He received the B.S. degree from the Beijing Institute of Technology, Beijing, China, in 1993, and the Ph.D. degree in electrical engineering from Tsinghua University, Beijing, in 2004.

He became a Professor and a Doctoral Tutor with Army Engineering University, Shijiazhuang, China, in 2009. He is currently a Professor with the China Army Engineering College. He is the author or coauthor of more than 100 scientific articles. His current research interests include vehicle maintenance and mechanical equipment test and fault diagnosis.

HONGBO FAN was born in Hubei, China, in 1982. He received the B.S., M.S., and Ph.D. degrees in mechanical engineering from the Ordnance Engineering College, Shijiazhuang, China, in 2004, 2007, and 2010, respectively.

He became an Engineer with the Department of Vehicle and Electrical Engineering, Army Engineering University, Shijiazhuang, in 2012. His current research interests include test technology and signal processing.

ZHINING LI was born in Shijiazhuang, China, in 1972. He received the B.S. and M.S. degrees in electrical engineering from Ordnance Engineering College, Shijiazhuang, China, in 1996 and 1999, respectively, and the Ph.D. degree in electrical and electronical from Tsinghua University, Beijing, China, in 2007.

He was a Postdoctoral Research Associate with the Ordnance Technology Research Institute, Shijiazhuang, China. In 2000, he joined Army Engineering University, Shijiazhuang, China, as an Assistant, where he was promoted to Associate Professor, in 2015. His current research interests include weak magnetic measuring and signal processing, fault diagnosis, and condition monitoring.